JOURNAL OF THERMOPHYSICS AND HEAT TRANSFER
Vol. 14, No. 1, January–March 2000

Experimental Analysis of Combusting Flows Developing over a Plane-Symmetric Expansion

M. Besson,* P. Bruel,† J. L. Champion,‡ and B. Deshaies§
Centre National de la Recherche Scientifique, 86961 Futuroscope Chasseneuil CEDEX, France

An experimental study of inert and combusting flows developing over a plane-symmetric expansion is presented. The flow under investigation consists of two fully developed turbulent channel flows of air (inert flows) or air plus propane (combusting flows) that are emerging just ahead of the sudden expansion. Such a flow geometry has been chosen to test turbulent combustion models that are able to take into account either a variable-mixture composition or (and) the simultaneous presence of large-scale coherent structures and stochastic turbulence. The present study concerns cases for which both streams have the same mass flow rate and the same equivalence ratio. The results put into evidence the asymmetry of the inert mean velocity field. The most striking effect of the presence of combustion is the symmetry brought to the mean flowfield and the related statistics accompanied by a deterministic pulsation of the reacting zones whose amplitude is governed by the characteristics of the reactants streams. Such a dramatic change in the flow properties represents a great challenge as far as computations of these flows are concerned.

Nomenclature

A_r	= area expansion ratio $[=(H_{\text{channel}} + 2h_{\text{step}})/H_{\text{channel}}]$
H_{channel}	= height of the inlet channels
h_{step}	= height of the steps at the sudden expansion
P_{atm}	= atmospheric pressure
$\langle p \rangle_{\text{wall}}$	= mean static wall pressure
Q_i	= mass flow rate of stream i
Re_{ch}	= Reynolds number $(U_{\text{axis}} H_{\text{channel}}/\nu_0)$
U_{axis}	= mean streamwise component of the velocity measured on the inlet channels centerline
U_{bulk}	= mean bulk velocity
(u, v)	= axial and normal components of the velocity
u_τ	= mean skin-friction velocity
(x, y)	= streamwise and normal coordinates
y_{lo}	= y ordinate of the lower wall of each of the two channels
y_{up}	= y ordinate of the upper wall of each of the two channels
y^*	= reduced y ordinate $[=(y - y_{\text{lo}})/(y_{\text{up}} - y_{\text{lo}})]$
ν_0	= kinematic viscosity of the incoming flow
Φ_i	= equivalence ratio of stream i

I. Introduction

ONE of the keys to the improvement of practical systems involving combustion in terms of both their efficiency and the reduction of their level of pollutant emission is a better understanding of the mechanisms of interaction between large-scale coherent structures and stochastic turbulence as well as the analysis of the influence of the combustion process on those mechanisms.

Emerging modeling techniques such as the large-eddy simulation[1] (LES) are aimed at better predicting such a kind of interaction by directly simulating the large scales while modeling the small ones by use of a subgrid scale (SGS) model. The development of a SGS model requires good knowledge of the dynamics of the energy transfer between the large-scale motion that is supposed to behave in a deterministic way and the stochastic turbulence that is controlling the small-scale motion. The predictive capabilities of such modeling techniques have to be tested on flow configurations that feature most of the phenomena present in real systems and whose boundary conditions are perfectly identified, not only for the average quantities (sufficient for the test of Reynolds-average-based models) but also for the instantaneous properties associated with these mean values. Among the various possible flow configurations that meet these requirements, those of bluff-body-stabilized flames[1–3] or those of flames stabilized by a sudden expansion[4–6] are the best candidates. As far as computations are concerned, the former configuration presents the drawback of requiring very fine meshes around the flame holder whereas the latter does not, as no body is needed to stabilize the combustion zone. Along these lines, the objective of this paper is to describe an experimental study devoted to the analysis of the main flow characteristics of inert and combusting flows over a plane-symmetric expansion. The unique feature of the rig is that the incoming flow consists of two streams of premixed reactants whose equivalence ratios can be different, thus allowing for the development of a mixing layer with an equivalence-ratio gradient. At each stage of the development of the rig, the concern of facilitating as much as possible the comparisons with computations was present.

II. Experimental Setup

An overview of the 10-m-long rig that has been developed, which is called ORACLES (for One Rig for Accurate Comparisons with Large-Eddy Simulations) is presented in Fig. 1. The rig includes four main sections: 1) two mixing chambers whose outlets are equipped with circular porous walls that will homogenize the air plus propane mixture and are followed by a converging section; 2) a 3-m-long section of constant rectangular cross section required for obtaining two fully developed turbulent channel flows upstream of the sudden expansion with turbulence characteristics as close as possible to equilibrium (to facilitate LES entrance conditions setting) as well as two-dimensional (in the width) mean flow characteristics (for conventional-model-based computations); 3) a 2-m-long combustion chamber thermally insulated (to allow for the use of isenthalpic combustion models) that incorporates windows placed along its length in pairs at opposite sides for both sidewalls and upper and lower walls; and 4) an exhaust section that follows the combustion chamber and is equipped with water-pressurized injectors. The fan of the extractor is powered by a 10-kW electric motor and is able to extract hot gases at a continuous rate of 3.5 m^3/s, exhausting them by means of a 6-m-high chimney (diameter 0.6 m).

Presented as Paper 99-0412 at the AIAA 37th Aerospace Sciences Meeting, Reno, NV, 11–14 January 1999; received 29 April 1999; revision received 22 July 1999; accepted for publication 22 July 1999.

*Graduate Student, Laboratoire de Combustion et de Détonique, 1 Avenue Clément Ader, ENSMA Téléport 2, BP 40109.

†Chargé de Recherche, Laboratoire de Combustion et de Détonique, 1 Avenue Clément Ader, ENSMA Téléport 2, BP 40109; bruel@lcd.ensma.fr.

‡Ingénieur de Recherche, Laboratoire de Combustion et de Détonique, 1 Avenue Clément Ader, ENSMA Téléport 2, BP 40109.

§Directeur de Recherche, Laboratoire de Combustion et de Détonique, 1 Avenue Clément Ader, ENSMA Téléport 2, BP 40109.

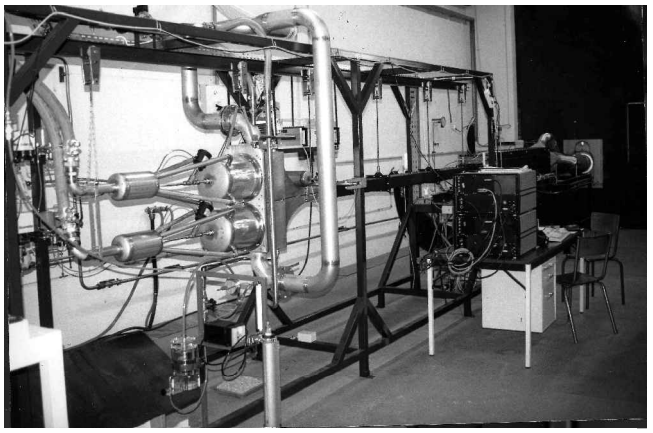

Fig. 1 Overview of the ORACLES rig.

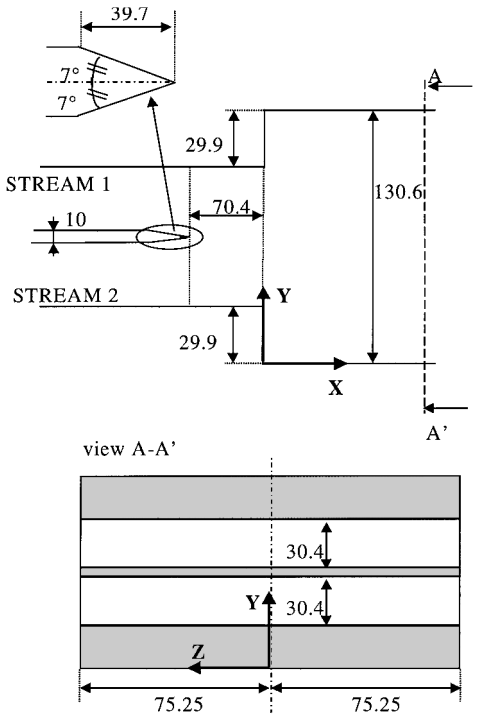

Fig. 2 Characteristic dimensions of the ORACLES rig (all dimensions in millimeters; uncertainty in dimensions = ± 0.5 mm).

The characteristic dimensions at the sudden expansion section are given in Fig. 2. A detailed view of the junction between the two inlet channels and the combustion chamber is presented in Fig. 3. The position of the end of the splitter plate has been chosen to avoid any flame's anchoring at its trailing edge. The fuel (commercial propane) and the air are supplied to the rig from high-pressure storage tanks. A chromatographic analysis of the fuel provides the following composition (in volume): 0.80% C_2H_6, 86.40% C_3H_8, 10.55% C_3H_6, and 2.25% C_4H_{10}, leading to the global formula $C_{3.015}H_{7.818}$. The basic quantities that characterize the flow are 1) the two mass flow rates Q_1 and Q_2, 2) the two equivalence ratios Φ_1 and Φ_2 based on the global definition of the fuel.

The mass flow rate per stream and the equivalence ratio can be varied between 0.05 and 0.2 kg/s and between 0.6 and 1.0, respectively. The temperature of each incoming stream, measured by thermocouples, is fixed by the different pressure drops through the air supply system and is equal to 273 ± 10 K.

Because of the long duration of the experiments, considerable attention has been paid to flow control to avoid as much as possible any mass-flow-rate and equivalence-ratio drifts. Thus a regulation loop is devoted to an Association des Ouvriers en Instruments de Précision (AOIP) central processor that is driving the mass-flow-rate

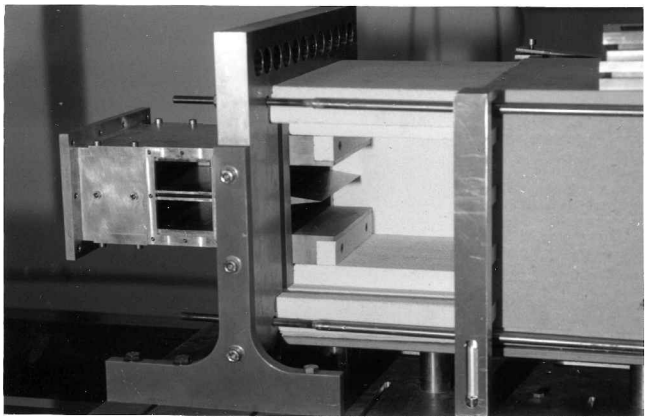

Fig. 3 Detailed view of the junction between the two-stream channel and the combustion chamber.

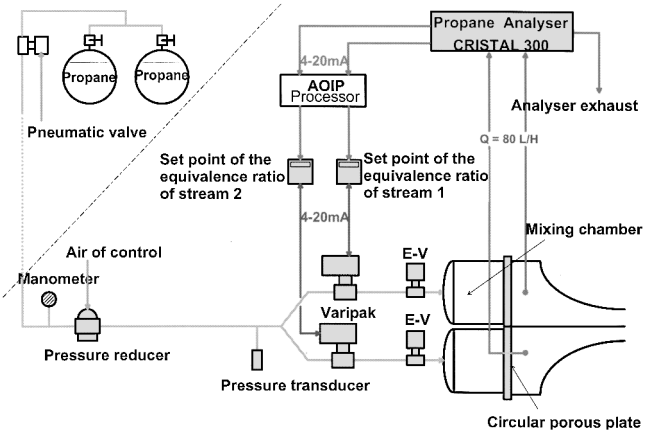

Fig. 4 Schematic of the gas supply lines and associated regulation system.

regulators that are controlling the air and gas valves such that Q_1 and Q_2 as well as Φ_1 and Φ_2 are maintained at their prescribed values during the duration of an experiment. The equivalence ratio of each incoming flow is continuously monitored by a Cosma Cristal 300 analyzer. A diagram of the gas regulation system is given in Fig. 4.

III. Measurement Equipment and Data Processing

A four-beam two-color laser Doppler velocimeter (LDV) is used for the velocity measurements. The beams are frequency shifted by Bragg cells to avoid any directional ambiguity. The flow is seeded with either vegetable oil (inert flows) or SiO_2 and TiO_2 particles (combusting flows). The two velocity components, (U for the axial X direction and V for the normal Y direction) are measured in the forward-scattering mode to maximize the signal-to-noise ratio. The scattered signal is collected by two photomultipliers, processed by two burst spectrum analyzers, and sent through an Institute of Electrical and Electronics Engineers (IEEE) 488 interface to a microcomputer for storage. The same microcomputer controls in real time, through a serial line, the system that displaces the three-axis LDV probe and the collecting optics. Taking into account the geometric characteristics of the effective measuring volume and of the displacement system, we estimate the systematic error in determining the location of the measuring volume is to be equal to ±0.5 mm. We evaluate the random errors by determining a 95% confidence interval by using the formulas given by Benedict and Gould.[7] The data processing used to obtain the various velocity moments and spectra is similar to the one described in detail by Sanquer et al.[2,3] and is not recalled here.

A row of static wall pressure probes is located on the external wall of each incoming channel. Connected to a water manometer, these probes provide the mean static wall pressure used to evaluate the

degree to which the channel flows are developed and subsequently to calculate the skin-friction velocity by

$$u_\tau = \sqrt{-0.5 H_{\text{channel}} \frac{1}{\rho} \frac{\partial \langle p \rangle_{\text{wall}}}{\partial x}}$$

Finally, direct light imaging of the combustion regions is performed by means of a video camera that provides 50 images per second with a time exposure per image that can be reduced down to 1/10,000 of a second. To improve the contrast of the images, the flow can be seeded with particles of $CuSO_4$ with the result of a greater light intensity of the seeded flame.

IV. Results

The main characteristics of the three selected cases considered in the following subsections are listed in Table 1. Case $i1$ corresponds to an isothermal flow, whereas cases $r1$ and $r2$ correspond to the combusting flows. The flow configurations have been chosen such that the flows in the two inlet channels possess characteristics as similar as possible. All of the measurements have been performed in the plane $z = 0$.

Incoming Flow Properties

The streamwise evolution of the mean static wall pressure measured along the external wall of the inlet channels is given in Fig. 5. At 1000 mm upstream of the sudden expansion, a quasi-linear pressure decrease is obtained that allows for the determination of the skin-friction velocity given in Table 1. The pressure balance between the two channels has proved to be relatively difficult to establish, and the slight difference observed between the pressure gradient in the two channels has been found impossible to reduce any further. A detailed analysis of both pressure and velocity measurements shows that both flows exhibit properties very close to those of a fully developed turbulent channel flow.

As far as the mean velocity profiles are concerned, Fig. 6 shows that the symmetry of the profiles with respect to each channel axis as well as the similarity between the velocity profiles of each stream is excellent, although the level of the velocity fluctuations is found to be slightly larger in the lower channel (stream 2) than in the upper one (stream 1). The similarity between the profiles in the two inlet channels is also observed for the instantaneous velocity histograms, as illustrated in Fig. 7 in which the streamwise velocity component histograms are plotted for both channels at the same y^* locations. The similarity between the morphologies of the u histograms appears to be satisfactory. Indeed, on the channel centerline ($y^* = 0.50$), a difference of less than 6% in the flatness factor f and less than 3% in the skewness factor s is obtained between the two channels. Closer to the wall ($y^* = 0.23$), these differences take values of 7 and 28%, respectively. The definitions of the skewness and flatness factors are

$$s = \frac{\overline{u'^3}}{(\overline{u'^2})^{\frac{3}{2}}}, \qquad f = \frac{\overline{u'^4}}{(\overline{u'^2})^2}$$

Table 1 Main parameters of the flows[a]

Case	Stream	Q, g/s	Re_{ch}	U_{axis}, m/s	U_τ, m/s	Φ
$i1$	1	52.8	24,556	12.0	0.54	——
	2	52.8	24,966	12.2	0.49	——
$r1$	1	52.8	24,556	12.0	0.54	0.65
	2	52.8	25,784	12.6	0.45	0.65
$r2$	1	52.8	25,989	12.7	0.54	0.85
	2	52.8	25,170	12.3	0.44	0.85

[a]Systematic error in $Q = \pm 1$ g/s, maximum random error in $U_{\text{axis}} = \pm 0.01$ m/s, maximum relative uncertainty in $U_\tau = \pm 6\%$, systematic error in $\Phi = \pm 0.025$.

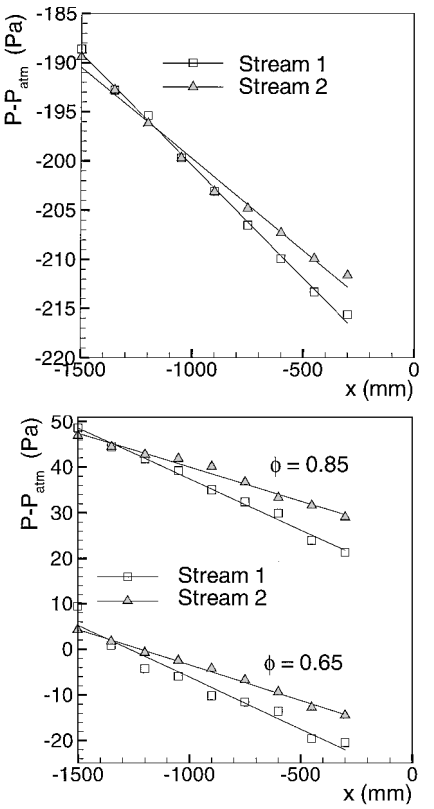

Fig. 5 Inert (top) and combusting (bottom) flows: evolution of the static wall pressure ($Q_1 = Q_2 = 52.8 \pm 1$ g/s; systematic error in P and $x = \pm 2$ Pa and ± 0.5 mm, respectively).

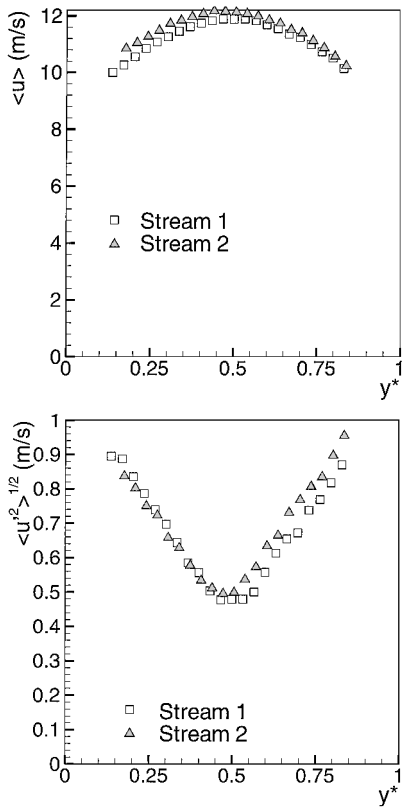

Fig. 6 Transverse profiles of the inlet streamwise mean (top) and fluctuating (bottom) velocity components at $x = -170 \pm 0.5$ mm ($Q_1 = Q_2 = 52.8 \pm 1$ g/s; maximum random error in $\langle u \rangle = 0.02$ m/s, systematic error in $y^* = \pm 0.02$).

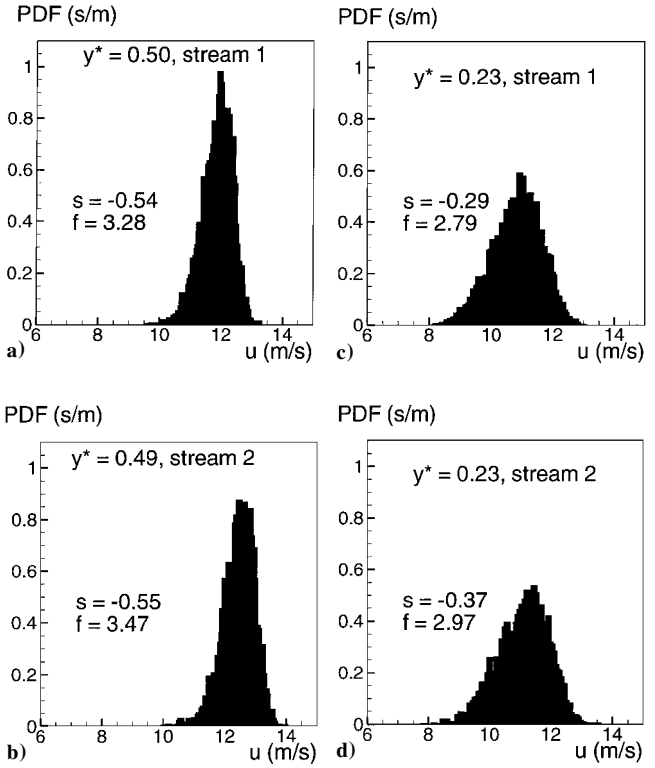

Fig. 7 Examples of histograms [probability density functions (PDFs)] of the streamwise-velocity component in the two inlet channels [$x = -170 \pm 0.5$ mm, $Q_1 = Q_2 = 52.8 \pm 1$ g/s; systematic error in $y^* = \pm 0.02$, velocity resolution and maximum relative uncertainty in histograms = a) 0.04 m/s and ± 4%, b) 0.04 m/s and 7%, c) 0.05 m/s and ± 3%, and d) 0.06 m/s and 4%].

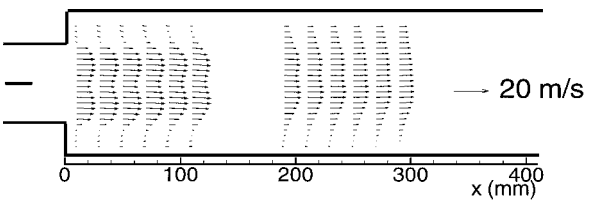

Fig. 8 Inert flow: measured mean velocity field ($Q_1 = Q_2 = 52.8 \pm 1$ g/s).

Flow Properties Behind the Sudden Expansion

Inert flow. The properties of inert flows behind sudden expansions have been extensively studied from both experimental and numerical points of view.[8–12]

In all these studies, only one stream emerged at the level of a single or a double backward-facing step. Abbott and Kline[8] show that in the case of a symmetric sudden expansion, the inert mean flow past the sudden expansion is asymmetric if the area expansion ratio A_r is greater than 1.5. In the present case of a two-stream incoming flow, A_r is equal to 1.84. The mean velocity field measured for the inert flow, case *i*1, is presented in Fig. 8 and several profiles of the two mean velocity components $\langle u \rangle$ and $\langle v \rangle$ are given in Fig. 9, in which the bulk velocity U_{bulk} has been calculated with the total mass flow rate, the incoming flow density and the area of the inlet channel at $x = 0$ mm. These figures show the asymmetry of the mean flow. In spite of the fact that the mesh of measurements points is relatively coarse and that no optical access is possible for x ranging from 115 to 185 mm, it clearly appears that the mean flow pattern is characterized by the presence of an upper mean recirculation zone that is much shorter than the one present in the lower part of the flow, in accordance with the findings of Abbott and Kline.[8] This asymmetry of the mean flow is consistent with the static pressure difference that exists between the two inlet flows (i.e., pressure level of stream 1 < pressure level of stream 2), which is evident in Fig. 5.

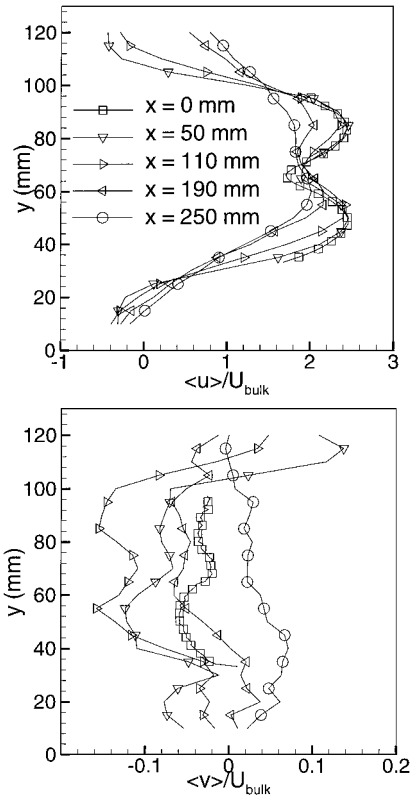

Fig. 9 Inert flow: profiles of the normalized mean streamwise (top) and normal (bottom) components of the velocity ($Q_1 = Q_2 = 52.8 \pm 1$ g/s, $U_{\text{bulk}} = 4.4 \pm 0.1$ m/s; systematic error in x and $y = \pm 0.5$ mm, maximum random error in $\langle u \rangle$ and $\langle v \rangle = \pm 5$ and ± 4%, respectively).

The mixing layer that is developing from $x = -70.4$ mm onward between the two channel flows is not found to modify the overall structure of the mean flow in the wakes of the two steps when compared with a one-stream sudden expansion. In the present experimental conditions involving the same mass flow rate in the two channels, the mixing layer exhibits only a slight velocity defect when its thickness becomes sufficient to allow for a direct interaction with the shear layers that are developing at the external boundary of the wakes of the two steps.

The presence of these shear layers is visible in the profiles of the rms velocity fluctuations presented in Fig. 10. A peak of fluctuations is observed on both components around $y = 30$ and 100 mm that corresponds to the location of the steps. The presence of the mixing layer creates also a local maximum for the velocity fluctuations around the symmetry axis of the combusting chamber (i.e., $y = 65.2$ mm) with the presence of a peak of fluctuations whose intensity level is much lower than those associated with the shear layers. As a consequence, it can be expected that, in the region of interaction between the shear layers and the mixing layer, the turbulent transport process is controlled mainly by the turbulence characteristics imposed by the steps' shear layers. However, the picture could be totally different if the two streams had different mass flow rates. Addressing this interesting issue by first studying the sensitivity of the shape of the recirculation zones to the initial slip velocity between the two incoming streams requires a finer mesh of measurements points and a parametric study that will be considered in a future work.

The asymmetry of the inert flow pattern is also visible in the histograms of the streamwise velocity component presented in Fig. 11 and obtained at points situated symmetrically at a distance of 40 mm from the centerline of the combustion chamber ($y = 65.2$ mm). At $x = 50$ mm, the morphology of the two histograms is clearly different whereas for $x = 290$ mm the histograms are similar but are centered around different values of the velocity in accordance with the differences observed between the flow patterns in the two regions. So the peculiarity of the structure of the present inert flow in

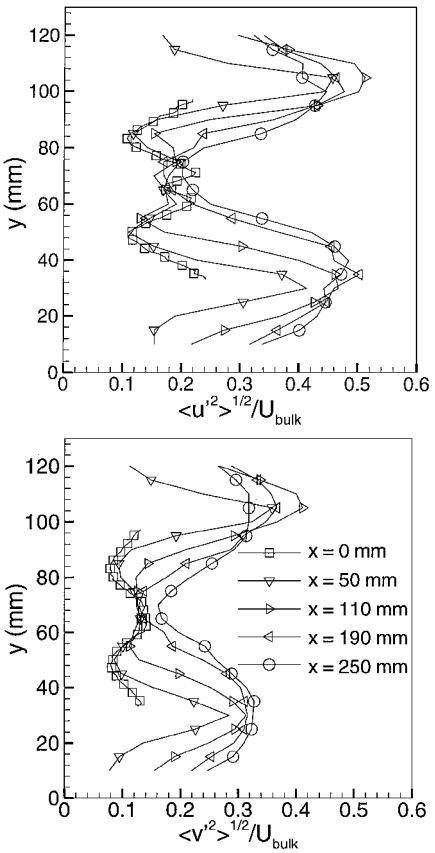

Fig. 10 Inert flow: profiles of the normalized rms longitudinal and normal velocity fluctuations ($Q_1 = Q_2 = 52.8 \pm 1$ g/s, $U_{bulk} = 4.4 \pm 0.1$ m/s; systematic error in x and $y = \pm 0.5$ mm, maximum random error in $\langle u'^2 \rangle^{1/2}$ and $\langle v'^2 \rangle^{1/2} = \pm 0.04$ and ± 0.03 m/s, respectively).

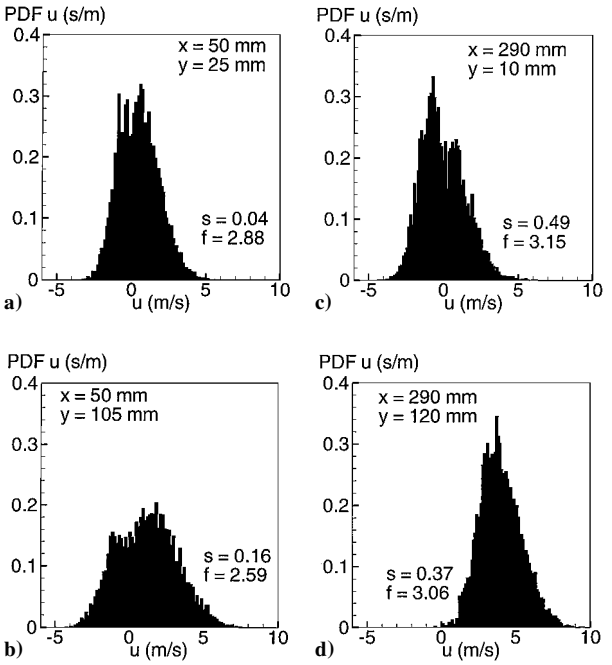

Fig. 11 Inert flow: histograms (PDFs) of the streamwise velocity components at points located symmetrically with respect to the centerline of the combustion chamber [$Q_1 = Q_2 = 52.8 \pm 1$ g/s; systematic error in x and $y = \pm 0.5$ mm, velocity resolution and maximum relative uncertainty in histograms = a) 0.11 m/s and ± 3.5%, b) 0.14 m/s and ± 2.5%, c) 0.12 m/s and ± 4%, and d) 0.10 m/s and ± 2.5%].

comparison with that of a bluff-body wake for comparable Reynolds number is as follows: 1) in the latter case the mean flow is axially symmetric, whereas the unsteady motion contains a periodic part that is not axially symmetric (vortex shedding), 2) in the present case, the mean flow and the related statistics are axially asymmetric and the unsteady flow motion does not exhibit an energetic periodic part. Thus the present isothermal flow configuration is well suited to test the versatility of LES approaches that have already been applied to simulate either inert and reacting bluff-body wakes[1] or flows in ramjet combustors.[13]

Combusting flows. The mean velocity field presented in Fig. 12 for case $r2$ appears to be radically different from its inert counterpart. Apart from the noticeable acceleration of the flow that takes place on both sides of the symmetry axis, the most important qualitative change in the mean velocity field of the combusting flow is its symmetry. Such a symmetry is illustrated in Fig. 13, which displays several profiles of the two mean velocity components for case $r1$. The symmetry of the mean flow is characterized by the symmetry of the $\langle u \rangle$ profiles and the antisymmetry of the $\langle v \rangle$ profiles, a feature that is also observed for the velocity profiles of case $r2$. For x varying between 0 and 250 mm, the central part of the flow, i.e., for y between

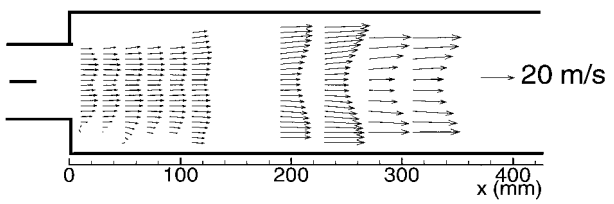

Fig. 12 Combusting flow: measured mean velocity field ($Q_1 = Q_2 = 52.8 \pm 1$ g/s, $\Phi_1 = \Phi_2 = 0.85 \pm 0.025$).

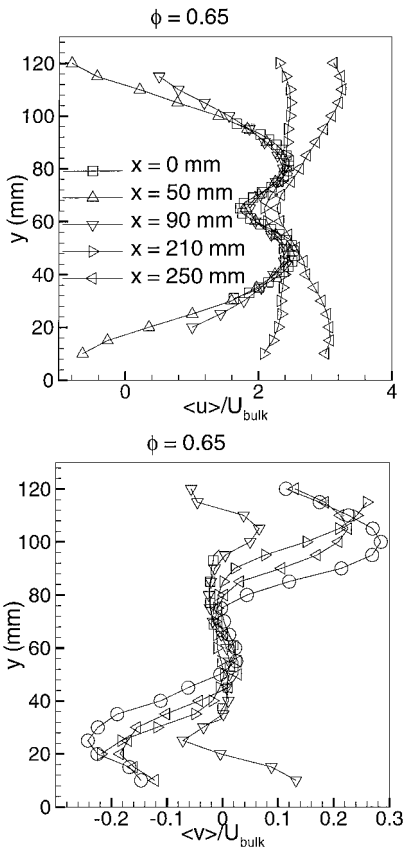

Fig. 13 Combusting flow: profiles of the normalized streamwise and normal mean components of the velocity ($Q_1 = Q_2 = 52.8 \pm 1$ g/s, $U_{bulk} = 4.4 \pm 0.1$ m/s, $\Phi_1 = \Phi_2 = 0.65 \pm 0.025$; systematic error in x and $y = \pm 0.5$ mm, maximum random error in $\langle u \rangle$ and $\langle v \rangle = \pm 0.06$ and ± 0.04 m/s, respectively).

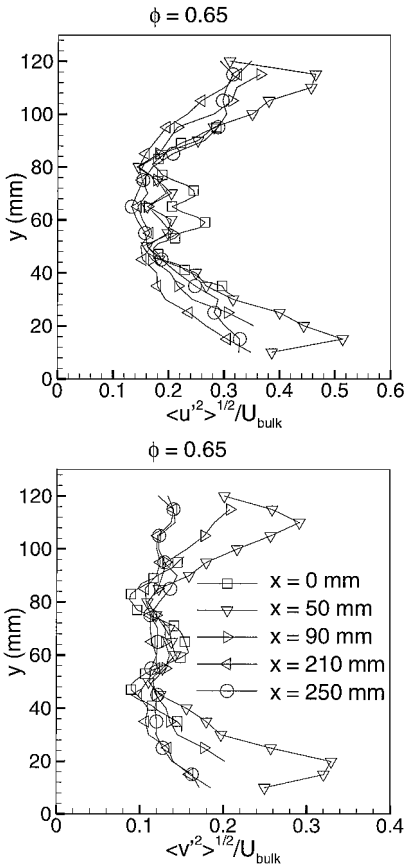

Fig. 14 Combusting flow: profiles of the normalized rms streamwise and normal velocity fluctuations ($Q_1 = Q_2 = 52.8 \pm 1$ g/s, $\Phi_1 = \Phi_2 = 0.65 \pm 0.025$, $U_{bulk} = 4.4 \pm 0.1$ m/s; systematic error in x and $y = \pm 0.5$ mm, maximum random error in $\langle u'^2 \rangle^{1/2}$ and $\langle v'^2 \rangle^{1/2} = \pm 0.04$ and ± 0.03 m/s, respectively).

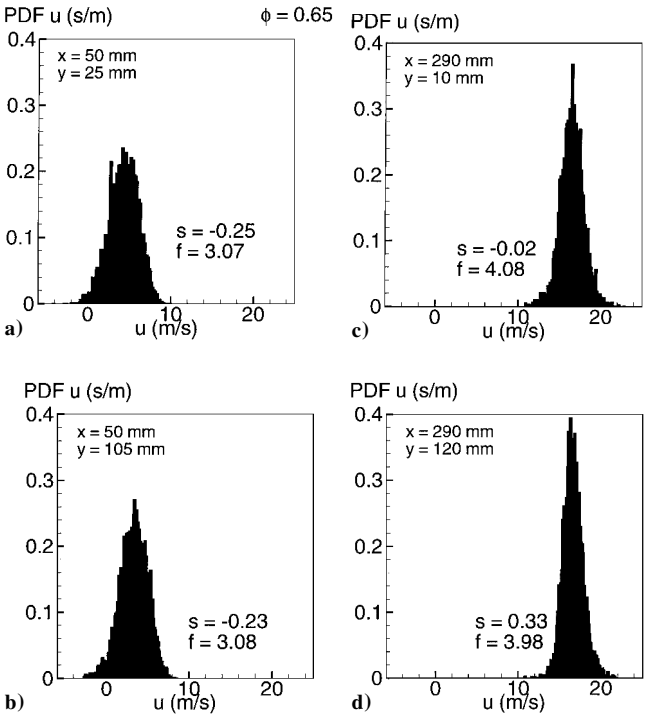

Fig. 15 Combusting flow: histograms (PDFs) of the streamwise velocity components at points located symmetrically with respect to the centerline of the combustion chamber [$Q_1 = Q_2 = 52.8 \pm 1$ g/s; systematic error in x and $y = \pm 0.5$ mm; velocity resolution and maximum relative uncertainty in histograms = a) 0.14 m/s and ± 4%, b) 0.11 m/s and ± 5%, c) 0.13 m/s and ± 1.5%, and d) 0.12 m/s ± 2.5%].

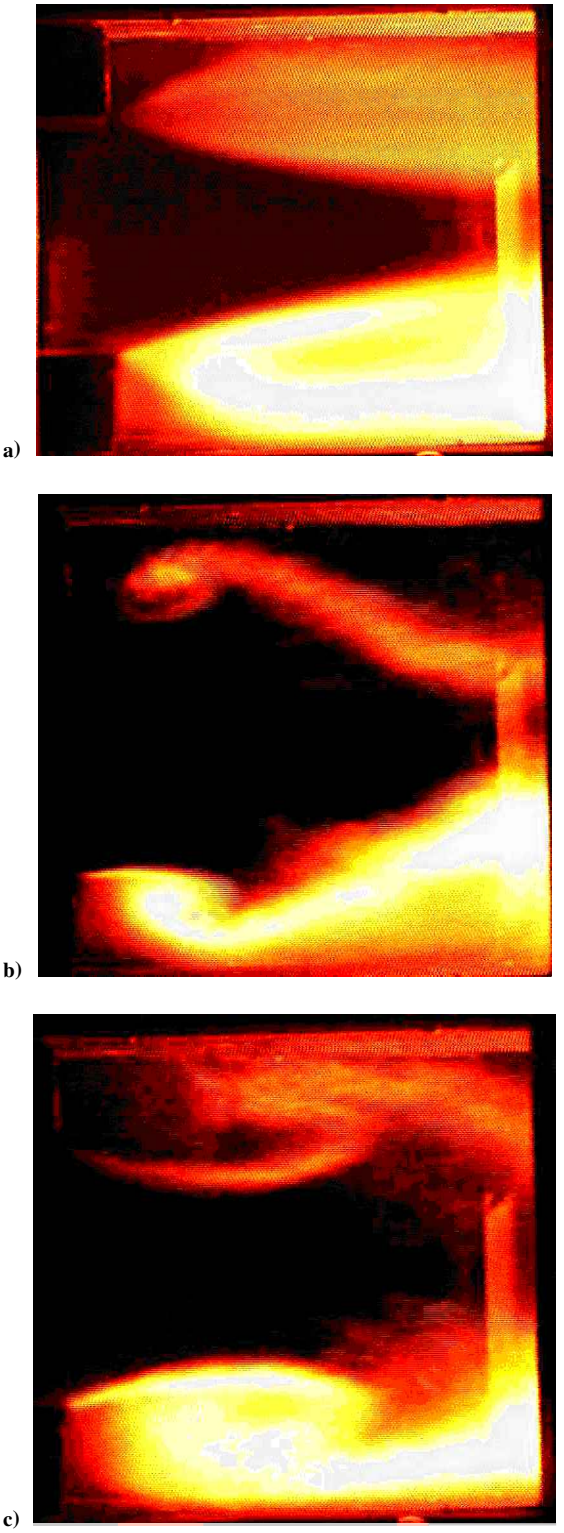

Fig. 16 Visualizations of the structure of the combusting flow just behind the sudden expansion ($Q_1 = Q_2 = 52.8 \pm 1$ g/s, $\Phi_1 = \Phi_2 = 0.85 \pm 0.025$): a) mean flow (time exposure 1/50 of a second); b) and c) examples of quasi-instantaneous flow patterns (time exposure 1/2000 of a second); the bottom flame is seeded with particles of $CuSO_4$.

40 and 90 mm, does not exhibit a significant flow acceleration, thus indicating that no significant combustion occurs in this region. In return, the flow regions close to the walls experience a strong flow acceleration with values of $\langle u \rangle$ that can be multiplied by more than a factor of 2 along the distance considered for the measurements and that is clearly related to the decrease in density that is due to combustion. As far as the velocity fluctuations presented in Fig. 14 are concerned, the influence of the presence of combustion is more

a question of shape of the profiles than of a change in the intensity level. Indeed, the important longitudinal gradients observed for both u' and v' in the inert case are not observed as soon as combustion is present. In addition, the location of the maximum values appears to be pushed toward the walls, and we observe a rapid decrease of these maxima as x increases. The symmetry of the mean combusting flow patterns finds its source in the symmetry of the statistical properties of the flow. Indeed, Fig. 15, which presents several histograms of u obtained at points placed at an equal distance (i.e., 40 mm) from the combustion chamber centerline, reveals that at $x = 50$ mm, a very good similarity between the histograms is obtained at $y = 25$ and 105 mm.

Farther downstream, at $x = 290$ mm, the histogram shapes are still alike, although some difference is obtained in the value of the skewness factor s. The flow visualizations presented in Fig. 16 provide a clear illustration of the symmetry that prevails in the mean and also, to some extent, in the unsteady part of the flow. The picture in Fig. 16a, obtained with a long time exposure, shows the mean flame brushes as a human eye can see them. Note that the location of the two mean flame brushes corresponds to the location of the

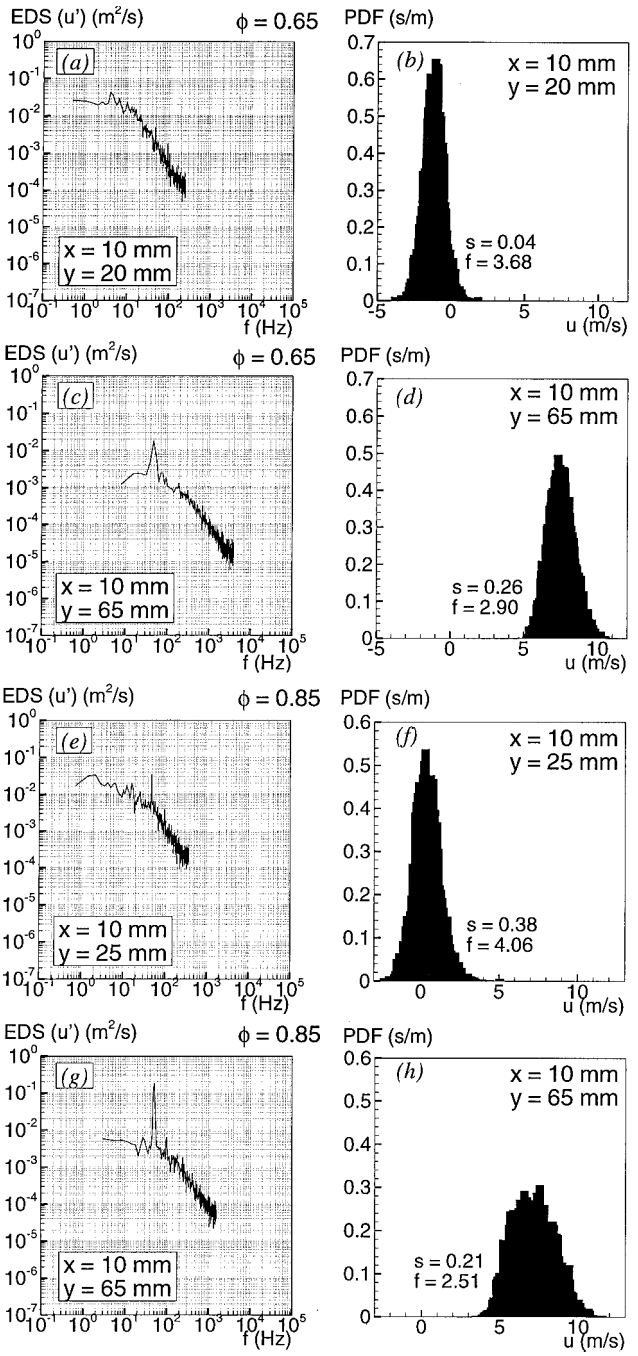

Fig. 17 Combusting flows: energy density spectra (EDS) and histograms (PDFs) of the streamwise components of the velocity: [$Q_1 = Q_2 = 52.8 \pm 1$ g/s, a)–d) $\Phi_1 = \Phi_2 = 0.65 \pm 0.025$ and e)–h) $\Phi_1 = \Phi_2 = 0.85 \pm 0.025$; systematic error in x and $y = \pm 0.5$ mm, maximum relative uncertainty in EDS = a) ± 1.5%, c) ± 0.5%, e) ± 1.4%, g) ± 0.7%; velocity resolution and maximum relative uncertainty in histograms = b) 0.07 m/s and ± 3.8%, d) 0.06 m/s and ± 3.3%, f) 0.10 m/s and ± 5.7%, h) 0.08 m/s and 1.3%].

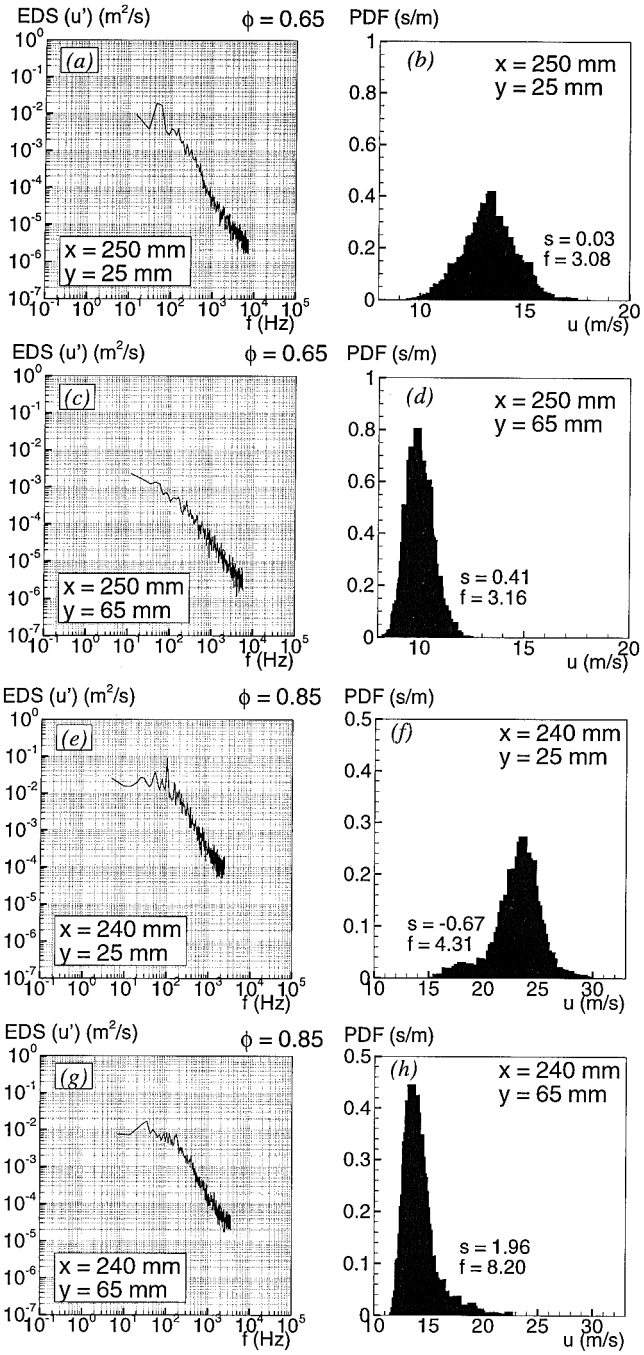

Fig. 18 Combusting flows: energy density spectra (EDS) and histograms (PDFs) of the streamwise components of the velocity ([$Q_1 = Q_2 = 52.8 \pm 1$ g/s, a)–d) $\Phi_1 = \Phi_2 = 0.65 \pm 0.025$ and e)–h) $\Phi_1 = \Phi_2 = 0.85 \pm 0.025$; systematic error in x and $y = \pm 0.5$ mm, maximum relative uncertainty in EDS = a) ± 7.8%, c) ± 12.5%, e) ± 2.4%, and g) ± 1.5%; velocity resolution and maximum relative uncertainty in histograms = b) 0.11 m/s and ± 5.6%, d) 0.09 m/s and ± 2.0%, f) 0.12 m/s and ± 1.2%, and h) 0.09 m/s and ± 6.5%].

strong flow acceleration observed in the profiles of $\langle u \rangle$ (Fig. 13). The dynamics of the two flame brushes can be observed when the time exposure is reduced (Figs. 16b and 16c): They appear to flap symmetrically, and the presence of vortical structures at the level of the two shear layers caused by the steps can be observed.

Note that this flame brush imaging, which uses the self-luminescence of the flame, is integrated over the whole width of the test section. The increase of the equivalence ratio between case $r1$ and case $r2$ with the same characteristics of the incoming flows renders the flapping of the brushes more vigorous. Such a pulsating behavior is well known for dump combustors, and a detailed review of the various related mechanisms of instability can be found in Ref. 14.

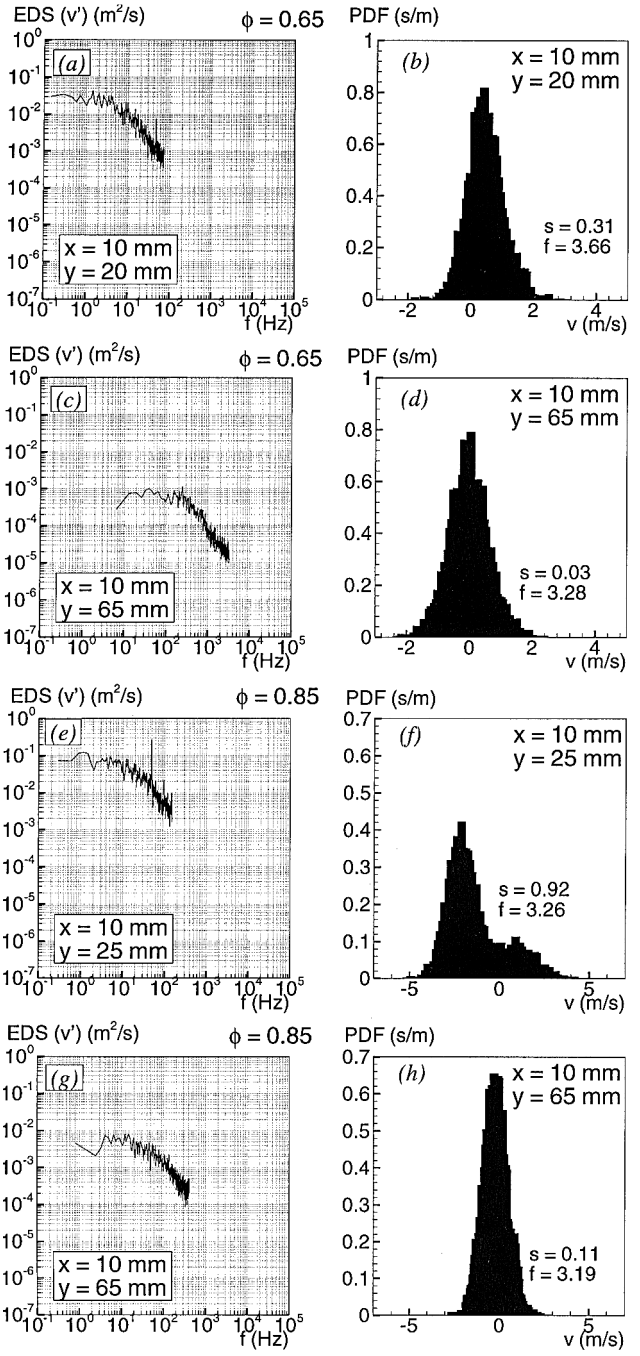

Fig. 19 Combusting flows: energy density spectra (EDS) and histograms (PDFs) of the normal components of the velocity [$Q_1 = Q_2 =$ 52.8 ± 1 g/s, a)–d) $\Phi_1 = \Phi_2 = 0.65 \pm 0.025$ and e)–h) $\Phi_1 = \Phi_2 = 0.85 \pm 0.025$; systematic error in x and $y = \pm 0.5$ mm, maximum relative uncertainty in EDS = a) ± 1.3%, c) ± 1.7%, e) ± 1.3%, g) ± 1.1%; velocity resolution and maximum relative uncertainty in histograms = b) 0.06 m/s and ± 6.4%, d) 0.05 m/s and ± 2.4%, f) 0.05 m/s and ± 6.6%, and h) 0.04 m/s and ± 2.3%].

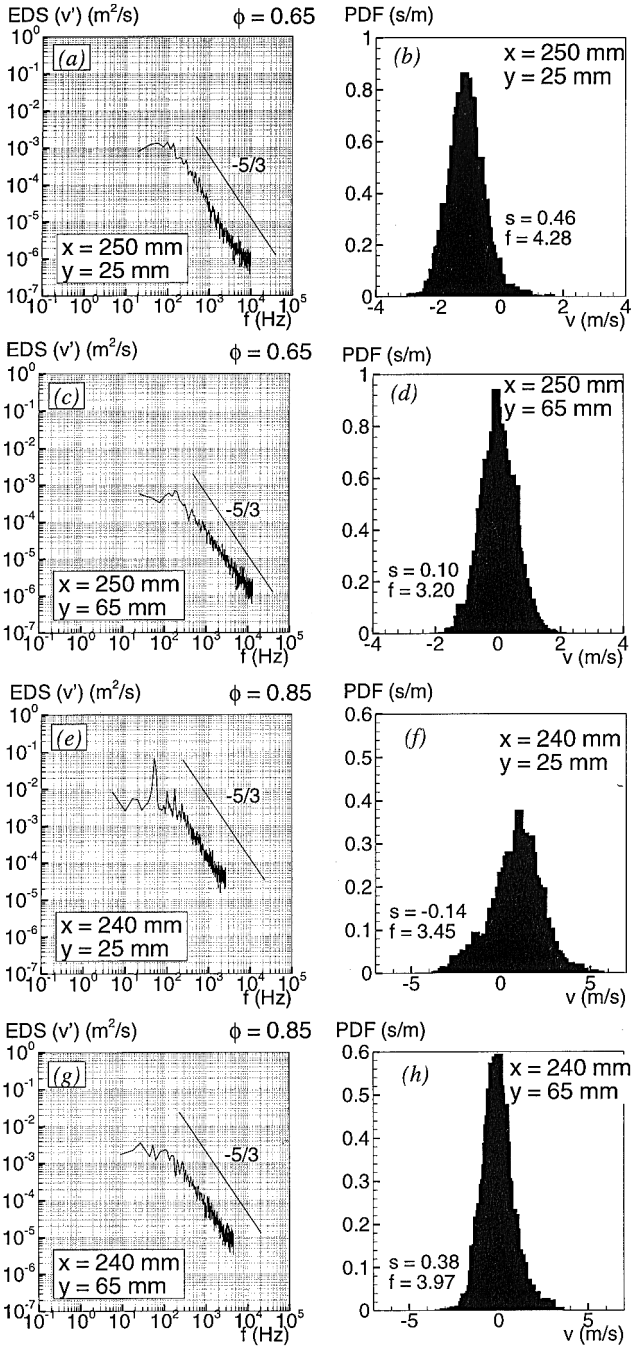

Fig. 20 Combusting flows: energy density spectra (EDS) and histograms (PDF) of the normal components of the velocity [$Q_1 = Q_2 =$ 52.8 ± 1 g/s, a)–d) $\Phi_1 = \Phi_2 = 0.65 \pm 0.025$ and e)–h) $\Phi_1 = \Phi_2 = 0.85 \pm 0.025$; systematic error in x and $y = 0.5$ mm, maximum relative uncertainty in EDS = a) ± 4.3%, c) ± 2.1%, e) ± 0.6%, and g) ± 0.8%; velocity resolution and maximum relative uncertainty in histograms = b) 0.07 m/s and ± 0.6%, d) 0.10 m/s and ± 1%, f) 0.09 m/s and ± 6.8%, and h) 0.11 m/s and ± 7.6%].

The analyses of the spectra of the streamwise and normal velocity components presented in Figs. 17–20 make it evident that the fundamental frequency associated with the brushes flapping is equal to 48.5 ± 2.5 Hz, with a harmonic of approximately 98.0 ± 2.5 Hz that is distinguishable on some spectra. It is important to note that the uncertainty about this typical frequency is representative of the dispersion of the values obtained only for different sets of measurements performed under the same conditions, and so are the uncertainty values given in the figure captions. The same frequency analysis applied to the inert flow does not show any remarkable frequency. The exact influence of the equivalence ratio on the energy associated with this pulsation is not clearly evident in these

figures and would require a specific analysis. Such a well-defined frequency appears in the spectra of both the streamwise (Figs. 17 and 18) and the normal (Figs. 19 and 20) velocity components. But, for the normal component, the signature of the pulsation is more clearly evidenced in the spectra corresponding to velocity measurements performed at the external boundary of the recirculation region ($y = 20$ and 25 mm). The damping of this specific frequency with the streamwise abscissa (i.e., from $x = 10$ to 250 mm) is more pronounced in the central part of the channel (i.e., $y = 65$ mm) than in the shear layers. It should be noted that the corresponding velocity histograms do not show well-defined bimodal shape, as obtained in the case of the vortex shedding that occurs in the inert wake of a bluff body.[3] Nevertheless, some asymmetry can be observed in the histograms for the largest value of the streamwise abscissa ($x = 250$ mm) in the case of the streamwise velocity component. Such an asymmetry is also observed for $x = 10$ mm for the normal velocity component, especially for the largest value of the equivalence ratio. In spite of the presence of a marked frequency, the spectra exhibit a classical behavior, namely a $-\frac{5}{3}$ power-law decay in their inertial range as was also observed for the velocity spectra of the inert flow.

V. Conclusion

As previously reported by other authors in the case of a one-stream sudden expansion, the inert mean and instantaneous flow patterns past the present two-stream sudden expansion are characterized by their asymmetry with respect to the combustion chamber centerline. Unlike the case of an inert wake behind a bluff body, the inert flow past the present sudden expansion does not show any distinguishable frequency on the velocity spectra. The most remarkable effect of the presence of combustion on the large-scale motion of the flow is to bring a quite perfect symmetry to the mean and, to some extent, to the unsteady flow patterns behind the sudden expansion. Moreover, the existence of marked frequencies on the velocity spectra shows the presence of a periodic component in the large-scale unsteady motion that is clearly related to the flame brush dynamics. Nevertheless, if a symmetric periodic behavior of the flame brush dynamics is observed for the large-scale motion, it can be expected, in view of the velocity spectra, that a stochastic behavior of the flame fronts exists at smaller scales. Visualizations by tomography as the ones provided by the use of planar laser-induced fluorescence that are needed to supplement the present description and enhance the understanding of the flame front behavior are presently in progress.

Acknowledgments

This study is supported by European Community Brite-Euram Project LES4LPP, Contract BRPR-CT95-0109 (DGXII-RSMT). Magali Besson has been granted a scholarship by Électricité de France, la Région Poitou-Charentes, and the Société Nationale d'Etude et de Construction de Moteurs d'Avion.

References

[1] Fureby, C., and Möller, S. I., "Large-Eddy Simulation of Reacting Flows Applied to Bluff-Body Stabilized Flames," *AIAA Journal*, Vol. 33, No. 12, 1995, pp. 2339–2347.

[2] Sanquer, S., Duplantier, S., Bruel, P., and Deshaies, D., "Similarity and Spectral Characteristics in the Turbulent Reactive Wakes of Bluff-Bodies," AIAA Paper 96-3034, July 1996.

[3] Sanquer, S., Bruel, P., and Deshaies, D., "Some Specific Characteristics of Turbulence in the Reactive Wakes of Bluff Bodies," *AIAA Journal*, Vol. 36, No. 6, 1998, pp. 994–1001.

[4] Shepherd, I. G., Moss, J. B., and Bray, K. N. C., "Turbulent Transport in a Confined Premixed Flame," *Proceedings of the 19th Symposium (International) on Combustion*, Combustion Inst., Pittsburgh, PA, 1982, pp. 423–431.

[5] Keller, J. O., Vaneveld, L., Korschelt, D., Hubbard, G. L., Ghoniem, A. F., Daily, J. W., and Oppenheim, A. K., "Mechanism of Instabilities in Turbulent Combustion Leading to Flashback," *AIAA Journal*, Vol. 20, No. 2, 1982, pp. 254–262.

[6] Ganji, A. R., and Sawyer, R. F., "Experimental Study of the Flowfield of a Two-Dimensional Premixed Turbulent Flame," *AIAA Journal*, Vol. 7, No. 7, 1980, pp. 817–824.

[7] Benedict, L. H., and Gould, R. D., "Towards Better Uncertainty Estimates for Turbulence Statistics," *Experiments in Fluids*, Vol. 22, No. 2, 1996, pp. 129–136.

[8] Abbot, D. E., and Kline, S. J., "Experimental Investigation of a Subsonic Turbulent Flow over Single and Double Backward-Facing Steps," *Journal of Basic Engineering*, Vol. 84, 1962, pp. 317–325.

[9] Durst, F., Melling, A., and Whitelaw, J. H., "Low Reynolds Number Flow over a Plane Symmetric Expansion," *Journal of Fluid Mechanics*, Vol. 64, No. 1, 1974, pp. 111–128.

[10] Mehta, P. R., "Separated Flow Through Large Sudden Expansion," *ASCE Journal of the Hydraulics Division*, Vol. 107, 1981, pp. 451–460.

[11] Gagnon, Y., Giovannini, A., and Hébrard, P., "Numerical Simulation and Physical Analysis of High Reynolds Number Recirculating Flows Behind Sudden Expansions," *Physics of Fluids A*, Vol. 5, No. 10, 1993, pp. 2377–2389.

[12] Armaly, B. F., Durst, F., Pereira, J. C. F., and Schönung, B., "Experimental and Theoretical Investigation of Backward-Facing Step Flow," *Journal of Fluid Mechanics*, Vol. 127, 1983, pp. 473–496.

[13] Menon, S., and Jou, W. H., "Large-Eddy Simulations of Combustion Instability in an Axisymmetric Ramjet Combustor," *Combustion Science and Technology*, Vol. 75, No. 1–3, 1991, pp. 53–72.

[14] Schadow, K. C., and Gutmark, E., "Combustion Instability Related to Vortex Shedding in Dump Combustors and their Passive Control," *Progress in Energy and Combustion Science*, Vol. 18, No. 2, 1992, pp. 117–132.